From the Eastern Vascular Society

Computer modeling for the prediction of thoracic aortic stent graft collapse

Salvatore Pasta, PhD,[a,b,c] Jae-Sung Cho, MD,[d,*] Onur Dur, PhD,[f] Kerem Pekkan, PhD,[f,g] and David A. Vorp, PhD,[b,c,d,e] *Palermo, Italy; Pittsburgh, Pa; and Istanbul, Turkey*

Objective: **To assess the biomechanical implications of excessive stent protrusion into the aortic arch in relation to thoracic aortic stent graft (TASG) collapse by simulating the structural load and quantifying the fluid dynamics on the TASG wall protrusion extended into a model arch.**

Methods: **One-way coupled fluid-solid interaction analyses were performed to investigate the flow-induced hemodynamic and structural loads exerted on the proximal protrusion of the TASG and aortic wall reconstructed from a patient who underwent traumatic thoracic aortic injury repair. Mechanical properties of a Gore TAG thoracic endoprosthesis (W. L. Gore and Assoc, Flagstaff, Ariz) were assessed via experimental radial compression testing and incorporated into the computational modeling. The TASG wall protrusion geometry was characterized by the protrusion extension (PE) and by the angle (θ) between the TASG and the lesser curvature of the aorta. The effect of θ was explored with the following four models with PE fixed at 1.1 cm: $\theta = 10$ degrees, 20 degrees, 30 degrees, and 40 degrees. The effect of PE was evaluated with the following four models with θ fixed at 10 degrees: PE = 1.1 cm, 1.4 cm, 1.7 cm and 2.0 cm.**

Results: **The presence of TASG wall protrusion into the aortic arch resulted in the formation of swirling, complex flow regions in the proximal luminal surface of the endograft. High PE values (PE = 2.0 cm) led to a markedly reduced left subclavian flow rate (0.27 L/min), low systolic perfusion pressure (98 mm Hg), and peak systolic TASG diameter reduction (2 mm). The transmural pressure load across the TASG was maximum for the model with the highest PE and θ, 15.2 mm Hg for the model with PE = 2.0 cm and $\theta = 10$ degrees, and 11.6 mm Hg for PE = 1.1 cm and $\theta = 40$ degrees.**

Conclusions: **The findings of this study suggest that increased PE imparts an apparent risk of distal end-organ malperfusion and proximal hypertension and that both increased PE and θ lead to a markedly increased transmural pressure across the TASG wall, a load that would portend TASG collapse. Patient-specific computational modeling may allow for identification of patients with high risk of TASG collapse and guide preventive intervention. (J Vasc Surg 2013;57:1353-61.)**

Clinical Relevance: **A potentially devastating complication that may occur after endovascular repair of traumatic thoracic aortic injuries is stent graft collapse. Although usually asymptomatic, stent graft collapse may be accompanied by adverse hemodynamic consequences. Numerous anatomic and device-related factors contribute to the development of collapse, but predictive factors have not yet been clearly defined. In the present study, we assessed the relevant hemodynamics and solid mechanics underlying stent graft collapse using a computational fluid-structure interaction framework of stent graft malapposition. Our findings suggest that both increased stent graft angle and extension into the aortic arch lead to a markedly increased transmural pressure across the stent graft wall, portending collapse. Patient-specific computational modeling may allow for identification of patients at high risk for collapse and aid in planning for an additional, prophylactic intervention to avert its occurrence.**

From the Fondazione Ri.MED, Palermo[a]; the Department of Bioengineering,[b] McGowan Institute for Regenerative Medicine,[c] Department of Surgery, Division of Vascular Surgery,[d] and Department of Cardiothoracic Surgery,[e] University of Pittsburgh, Pittsburgh; the Department of Biomedical Engineering, Carnegie Mellon University, Pittsburgh[f]; and the Department of Mechanical Engineering, Koc University, Istanbul.[g]

*Current affiliation: Loyola University Chicago Stritch School of Medicine, Maywood, Ill.

Author conflict of interest: none.

Presented at the Twenty-fifth Annual Meeting of the Eastern Vascular Society, National Harbor, Md, September 22, 2011.

Reprint requests: David A. Vorp, PhD, 412 Center of Bioengineering (CNBIO), University of Pittsburgh, 300 Technology Dr, Pittsburgh, PA 15219 (e-mail: vorp@pitt.edu).

The editors and reviewers of this article have no relevant financial relationships to disclose per the JVS policy that requires reviewers to decline review of any manuscript for which they may have a conflict of interest.

0741-5214/$36.00

http://dx.doi.org/10.1016/j.jvs.2012.09.063

Thoracic endovascular aortic repair (TEVAR) has emerged over the last decade as the preferential minimally invasive treatment for various thoracic aortic pathologies including traumatic thoracic aortic injuries (TTAI).[1-4] Although TEVAR for TTAI is effective, its durability remains a concern, especially in young patients.[5,6] Applications outside of physical conditions for which the thoracic aortic stent graft (TASG) was designed could result in device failure,[7] which may lead to distal end-organ malperfusion caused by aortic occlusion, endoleak, and reperfusion of the injured aorta or endograft infolding or collapse. Physiologic aortic coarctation and partial or total endograft collapse are the most common complications, although these occur rarely.[3,8-12] Collapse occurs relatively early in the postoperative period with nearly all patients presenting

within 3 months,[13,14] but cases of late collapse have also been reported.[11,15]

Numerous anatomic and device-related factors contribute to stent graft collapse, including a young healthy aorta with tight aortic arch, a narrow aortic diameter, excessive endograft oversizing, a "bird beak" effect, low radial force of endografts, and material fatigue.[10] The incidence rates of stent graft collapse after TEVAR for TTAI are not well defined.[10,14] Although usually asymptomatic, collapse may be accompanied by devastating hemodynamic consequences, requiring a secondary intervention by means of redo TEVAR or conversion to open surgery, with attendant morbidity and mortality.[10,15] Endograft collapse–related mortality rates of 16.9% for asymptomatic patients and 27.3% for symptomatic patients within 3 years of diagnosis have been reported.[7,11,12,14-17] Collapse is most often observed when the proximal extent of a TASG is in the transverse arch with malapposition of the TASG along the lesser curvature of the aorta (the so-called "bird beak" phenomenon).[11,12,14,15,17]

Although the "bird beak" effect is often observed after TEVAR of TTAI, hemodynamic disturbances or collapses do not occur in all cases. It is desirable to identify patients at the highest risk for developing such complications so that a prophylactic intervention can be undertaken after the patient has recovered from the initial trauma before such complications occur.[11,15] However, predictors of these complications have not been defined yet. To identify the predictors, we developed a computational fluid-structure interaction (FSI) framework of TASG malapposition. This modeling technique is emerging as a practical tool, at a level of detail impossible with experimental techniques, for investigatingmultiphysics phenomena involving the interaction of a flowing fluid (eg, blood) with flexible structures (eg, both aorta and endograft).[18] We hypothesize that malapposition can result in increased hemodynamic loads on the graft that may reach sufficient magnitude to cause gradual infolding of the TASG and even collapse. This hypothesis was assessed by evaluating the relevant fluid dynamics and mechanical forces exerted on and consequent TASG deformation in several realistic but geometrically distinct models of TASG malapposition with protrusion into the aortic arch. Specifically, the influence of varying degrees of TASG angulation and protrusion extension were investigated.

METHODS

Three-dimensional aortic and thoracic aortic stent graft geometry. The three-dimensional aortic arch geometry created in our model was segmented from computed tomography data using the vascular modeling toolkit VMTK v0.9.0 (http://www.vmtk.org). Specifically, the aorta in a male patient who underwent a TEVAR for a TTAI and subsequently developed endograft collapse with neurologic complications was reconstructed. This case has previously been reported by Shukla et al.[11] The three-dimensional anatomy was modeled from the aortic valve, through the ascending aorta, aortic arch, supra-aortic vessels (ie, innominate artery, left common carotid artery, left subclavian artery [LSA]), and descending aorta, ending at the level of the diaphragm.

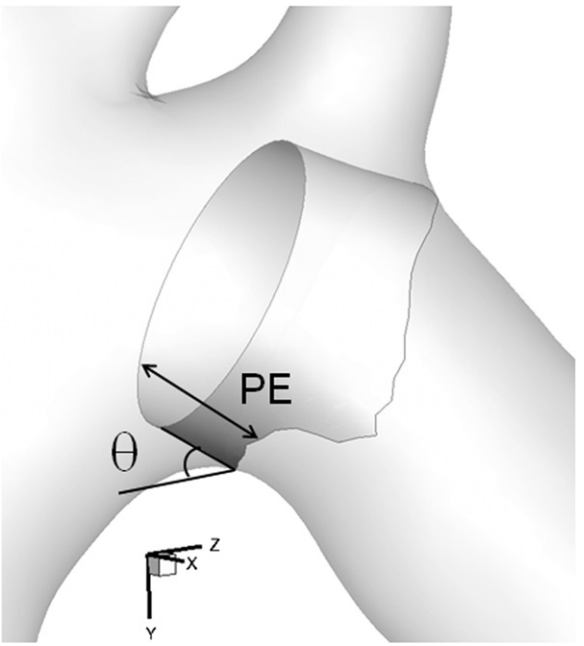

Fig 1. View of the thoracic aortic stent graft protrusion (model with protrusion extension [*PE*] = 1.1 cm and θ = 10 degrees) placed into the aortic arch model and schematic representation of the geometric parameters used to define the protrusion geometry.

The complex geometry of the Gore TAG endograft (W. L. Gore and Assoc, Flagstaff, Ariz) was extracted from the same patient's computed tomography scan and modeled parametrically as a tubular protrusion into the aortic arch. The protrusion geometry was defined by two parameters: (1) the protrusion extension (PE), defined as the length of TASG protrusion not in contact with the aortic wall, and (2) the angle (θ) between the lesser curvature of the aorta and the protruded segment of the TASG wall (Fig 1). Both geometric parameters consider the influence of the "bird beak" phenomenon by its PE and angulation. The PE was placed into the three-dimensional model as it appeared in the computed tomography images of the patient after TTAI repair, using the surgical planning and anatomic editing tools.[19]

A parametric analysis of TASG wall protrusion was carried out by individually varying the PE and θ parameters. To explore the effects of θ, we evaluated the following four models with PE fixed at a value of 1.1 cm: θ = 10 degrees, 20 degrees, 30 degrees, and 40 degrees. The effects of PE were explored with three additional models (besides PE = 1.1 cm) with θ fixed at 10 degrees: PE = 1.4 cm, 1.7 cm, and 2.0 cm. None of these models occluded the LSA completely. A model without a TASG was also studied for comparison.

Computational fluid-structure interaction analysis. One-way coupled FSI analyses were performed to explore the relevant fluid dynamics, mechanical forces, and

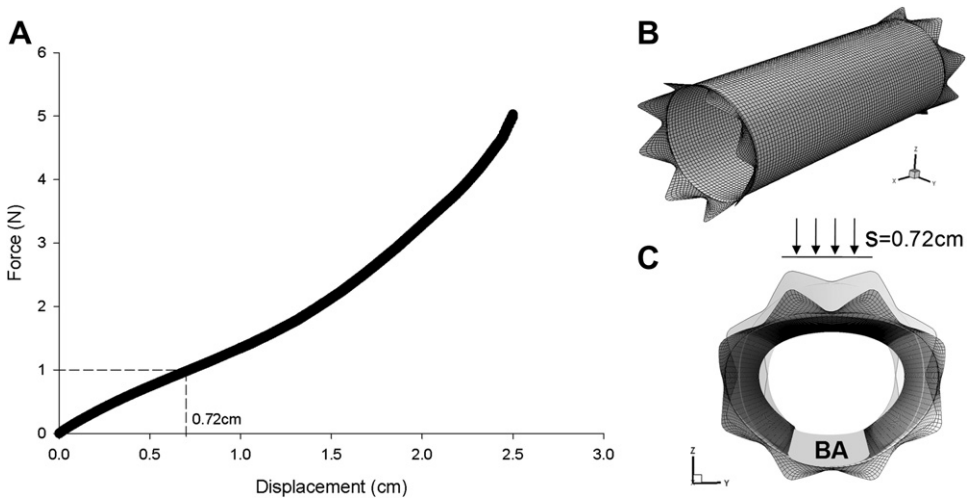

Fig 2. A, Experimentally derived force vs displacement curve of a Gore TAG endoprosthesis under radial compression testing. **B,** Computational mesh of thoracic aortic stent graft model used to simulate radial compression testing. **C,** Deformed (*meshed solid model*) and undeformed (*gray solid model*) geometry of thoracic aortic stent graft under compression displacement of 0.72 cm showing the boundary area (*BA*) where reaction force was evaluated.

deformation inducing TASG collapse. Discretization of both fluid and solid domains was accomplished with approximately 2 million unstructured tetrahedral elements using GAMBIT 2.3.6 (ANSYS Inc, Canonsburg, Penn) software.[20]

Fluid simulations. The hemodynamic loads on the protruded TASG and aortic wall were estimated using steady and unsteady fluid dynamic simulations using FLUENT v13.0.0 (ANSYS Inc). The computational fluid dynamic (CFD) model is based on an experimentally validated second-order algorithm that is specifically developed to resolve high-frequency, time-dependent flow instabilities encountered in complex cardiovascular anatomies.[19-21] As in other aortic flow studies,[19-22] the blood flow was assumed incompressible and Newtonian with a density of 1060 kg/m^3 and viscosity of 3.71×10^{-3} Pa $\times$ s. This is a valid assumption in large artery models. The aortic wall and TASG wall protrusion were assumed as rigid and impermeable. The continuity equation and the linearized momentum equation were solved sequentially using a segregated algorithm. Convergence was enforced by reducing the residual of the continuity equation by 10^{-7} at all time steps.

The total cardiac output (ie, inlet flow to aortic root) was assumed at 5L/min, and this flow was distributed between the supra-aortic vessels and the descending aorta with a ratio of 40:60 (corresponding to in vivo patient measurements) using resistance boundary conditions.[20] Steady-state solutions were used to initiate the flow field before the transient analyses. During CFD simulation, the pressure gradient calculated at the outlets was attenuated 10 times to ensure smoother convergence. Each downstream resistance was coupled to the solver iteratively to prevent divergence owing to multiple outlets.[19] A patient-specific pulsatile aortic flow waveform[22] was used as the inlet conditions for the unsteady CFD simulations. Simulations were continued through six cardiac cycles to eliminate nonlinear start-up effects. After solution convergence, the mesh of the aortic wall and TASG protrusion as well as hemodynamic forces (ie, pressure, viscous, and surface tension forces) at each node were exported for the subsequent structural analyses.

Thoracic aortic stent graft mechanical properties evaluation. Radial compression testing was performed to evaluate experimentally the stiffness of a Gore TAG endoprosthesis for inclusion in the FSI model. The stent graft (26-mm diameter) was placed between two closely positioned, firm, smooth-surface grips in a universal material testing system (model 5542A; Instron, Norwood, Mass) with a 5-kN load cell. A constant crosshead speed of 0.1 cm/min was applied to compress the TASG gradually in the radial direction. Fig 2, *A*, shows the force vs displacement curve of the radial compression test on the endograft.

Computational finite element analysis was performed to simulate the radial compression test and to determine iteratively the TASG mechanical properties by comparison with the experimental data in Fig 2, *A*. Specifically, the geometry of the stent graft was generated and meshed using quadrilateral structural elements in ABAQUS v.6.11 (SIMULIA Inc, Providence, RI) software (Fig 2, *B*). The TASG was modeled as a homogeneous shell with linear elastic material properties. The thickness of the endograft was 0.09 cm, whereas the Poisson ratio was assumed to be 0.3, which is the representative value of the endograft-related nitinol scaffold. The nodes along the bottom of the TASG were constrained in all directions to simulate firm support, and a displacement value of 0.72 cm (corresponding to 1-N load) was applied to the nodes along the top of the TASG (Fig 2, *A* and *C*). The stiffness of the TASG was

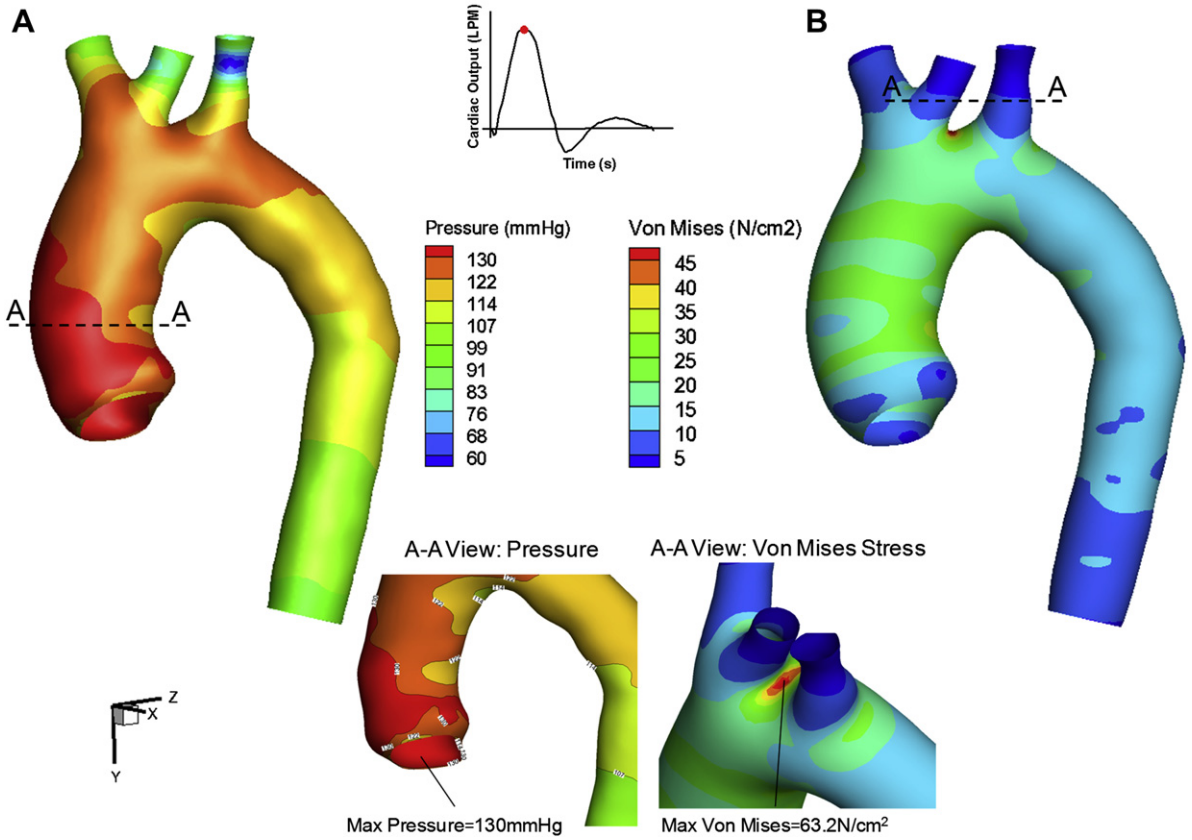

Fig 3. A, Map of pressure distribution of aortic model without thoracic aortic stent graft at peak systolic. **B,** Distribution of von Mises wall stress induced by hemodynamic loads at peak systole. View (*A-A*) on center bottom displays maximum value of peak systolic pressure and von Mises wall stress.

adjusted iteratively until the simulation revealed the reaction force (1 ± 0.02N obtained after six iterations) that was measured in the experimental radial compression test. A TASG stiffness of 840 N/cm^2 was estimated by this analysis, a value consistent with earlier studies.[23,24]

Structural simulations. Structural analyses were performed using ABAQUS FE software (SIMULIA Inc) to assess the stress distribution and deformation induced by hemodynamic loads. The geometries and meshes of both the TASG and the aorta were imported as homogeneous shells (scale 1:1) with consequent mesh degeneration into three-node triangular elements. The TASG was taken as 0.9 mm thick, whereas the aortic wall was assumed to be 1.72 mm.[25] The hemodynamic forces exported by CFD analyses were applied at each node of the structural model. The aorta was assumed to be a hyperelastic, homogeneous, incompressible, and isotropic material using a finite strain constitutive model developed previously by our laboratory for modeling the human aorta.[26] The TASG body was modeled as a linear-elastic material with stiffness of 840 N/cm^2 and Poisson ratio of 0.3 as previously measured. Material nonlinearities owing to large deformation were considered. For the aorta to deform in a physiologic manner, the distal ends of the supra-aortic vessels, aortic valve, and descending aorta were fixed in all directions and sufficiently extended. Tie contact conditions, which allow us to constrain together the dissimilar element nodes of the TASG and aortic wall, were adapted to fix the interface of the TASG wall protrusion to the aortic wall.

RESULTS

Fig 3, *A*, shows the detailed distribution of blood pressure at peak systole for the aortic model without an endograft. High-pressure values were found in the proximal ascending aorta with a maximum of 124.9 mm Hg corresponding to the aortic valve inlet. The effect of hemodynamic forces on the aortic wall stress distribution is measured in terms of von Mises stress, which is an index especially suited for failure analysis (Fig 3, *B*). A maximum stress value of 63.2 N/cm^2 was found in the aortic arch distal to the ostia of the supra-aortic vessels. Peak systolic pressure into the LSA for this case was approximately 116 mm Hg.

Hemodynamic characteristics with and without TASG are illustrated using streamlines (Fig 4). At peak systole, streamlines run parallel to the aortic wall in the absence of

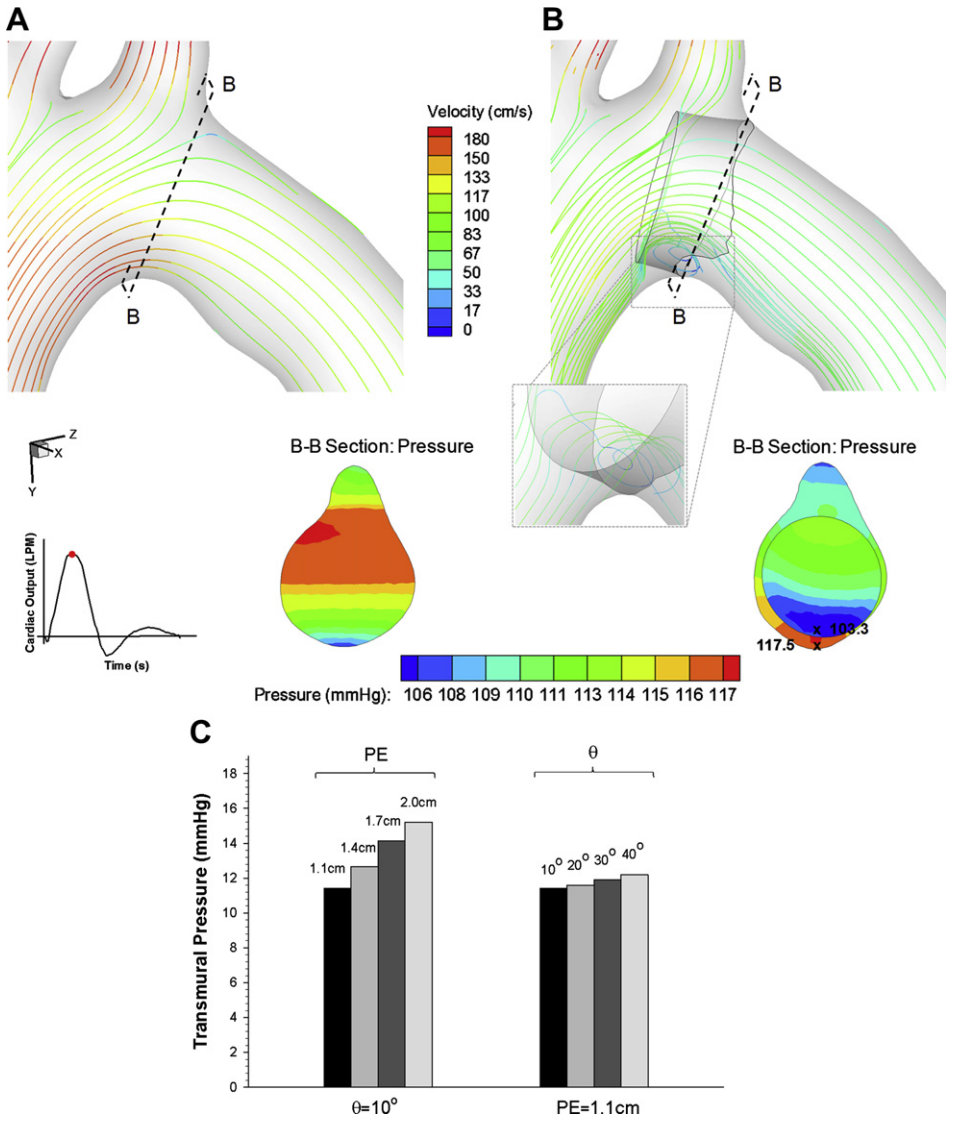

Fig 4. **A** and **B,** Streamlines of blood flow velocity in aortic model without a thoracic aortic stent graft (TASG) **(A)** and with a TASG **(B)** (protrusion extension [*PE*] = 1.1cm and θ = 10 degrees) at peak systole. The cross sections *B-B* (*inset in the bottom*) show the peak systolic pressure in a cross section of the aorta with and without TASG. **C,** Transmural pressure gradient across the TASG wall protrusion for all geometries at cross section B-B.

the stent graft (Fig 4, *A*), but those close to the protruded TASG lost this characteristic laminar pattern (Fig 4, *B*). The malapposed endograft generates vortices in the proximal luminal surface of the endograft close to the tight aortic arch. Additionally, a cross section of the endograft (see *inset* of Fig 4, *B*) reveals that a transmural pressure load difference exists between the undersurface and the luminal surface of the malapposed TASG that would likely portend TASG infolding or collapse. A summary of transmural pressure gradients for all examined combinations of PE and angulation parameters is shown in Fig 4, *C*. The model with greatest PE (ie, PE = 2.0 cm and θ = 10 degrees) exhibited the maximum transmural pressure gradient of 15.2 mm Hg, which is higher than that shown by the model with greatest θ (11.6 mm Hg for PE = 1.1 cm and θ =40 degrees).

Wall stress distribution and streamlines of blood velocities were investigated at three different phases of the cardiac cycle for the model with PE = 2.0 cm and θ = 10 degrees (Fig 5, *A*). During acceleration, the antegrade blood flow increases gradually and generates a pressure load on the TASG wall that deforms the stent graft gradually inward toward the lumen of the aorta. This infolding reaches its maximum deformation at peak systole, where the TASG protrusion exhibits the highest wall stresses. During deceleration (ie, late systole), the wall stress on the TASG diminishes such that it resumes its original position and shape. These hemodynamic loads determined the degree of

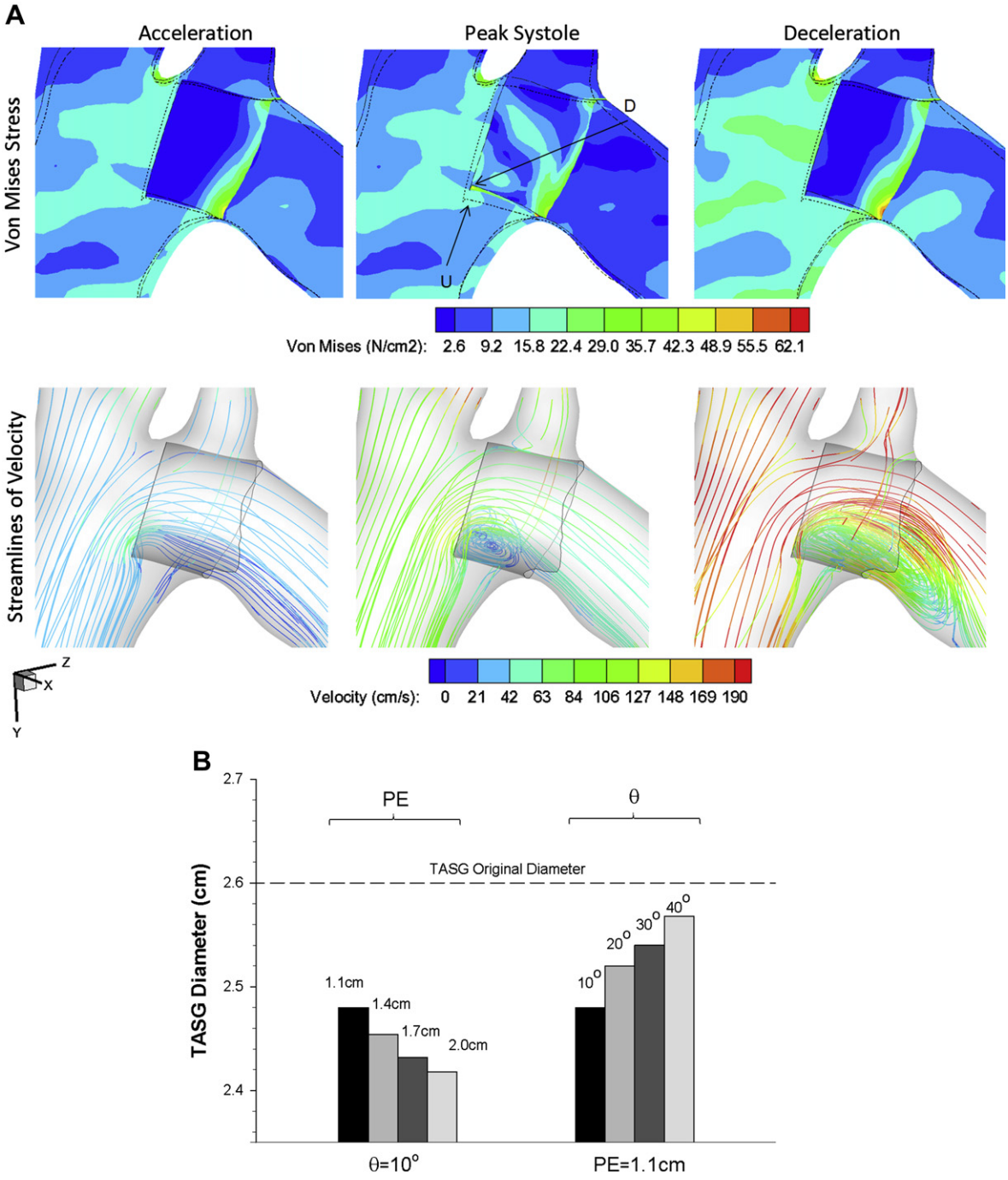

Fig 5. A, Distribution of von Mises stress and streamlines of blood velocity during acceleration, peak systole, and deceleration for the model with protrusion extension (*PE*) = 2.0 cm and θ = 10 degrees. The tip of the thoracic aortic stent graft in the deformed model (*D*) shows infolding compared withthe undeformed model (*U*), whereas vortices of blood velocity streamlines increase significantly during deceleration. **B,** Thoracic aortic stent graft diameter at peak systole for all geometries.

compression of the TASG at peak systole (Fig 5, *B*). The TASG diameter decreases with PE up to a minimum of 24 mm for the model with PE = 2.0 cm and θ = 10 degrees, whereas the model with different θ showed moderate diameter reduction (25.6 mm for PE = 1.1 cm and θ = 40 degree). The streamlines of blood velocity over the cardiac cycle display an increasing number of vortices becoming more complex at the deceleration phase.

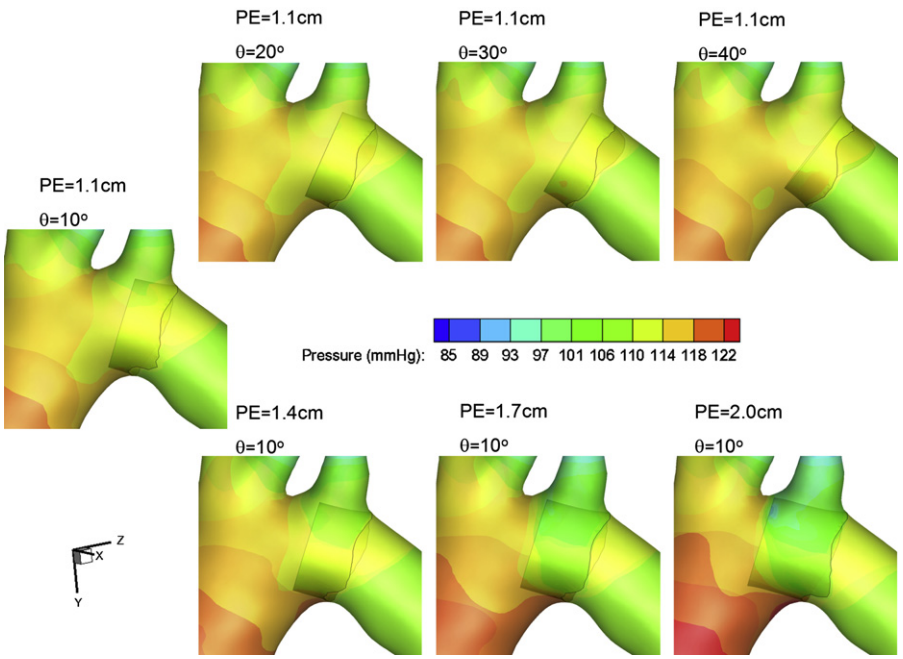

Fig 6. Distribution of luminal pressure for all aortic models with different geometries of thoracic aortic stent graft wall protrusion at peak systole. *PE*, Protrusion extension.

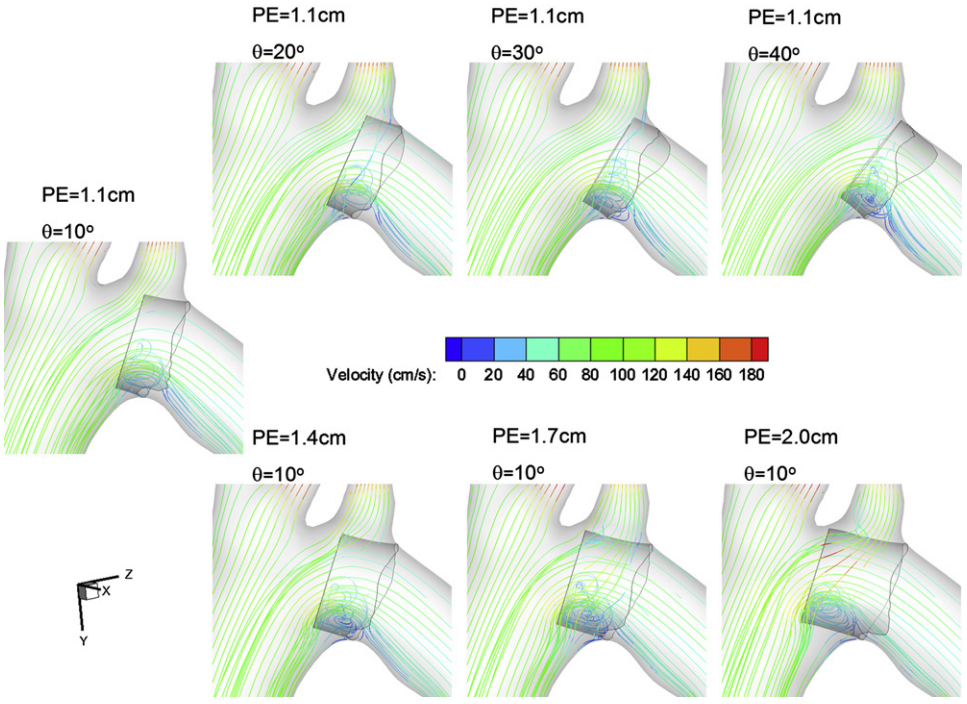

Fig 7. Streamlines of blood flow velocity for all aortic models with different thoracic aortic stent graft wall protrusions at peak systole. *PE*, Protrusion extension.

Fig 6 displays the comparison of pressure distribution for all models with different TASG wall protrusion geometries. Peak systolic pressure in the proximal aortic arch was found to increase as both geometric parameters increased; this effect is more pronounced with higher PE (bottom three models in Fig 6) compared with higher

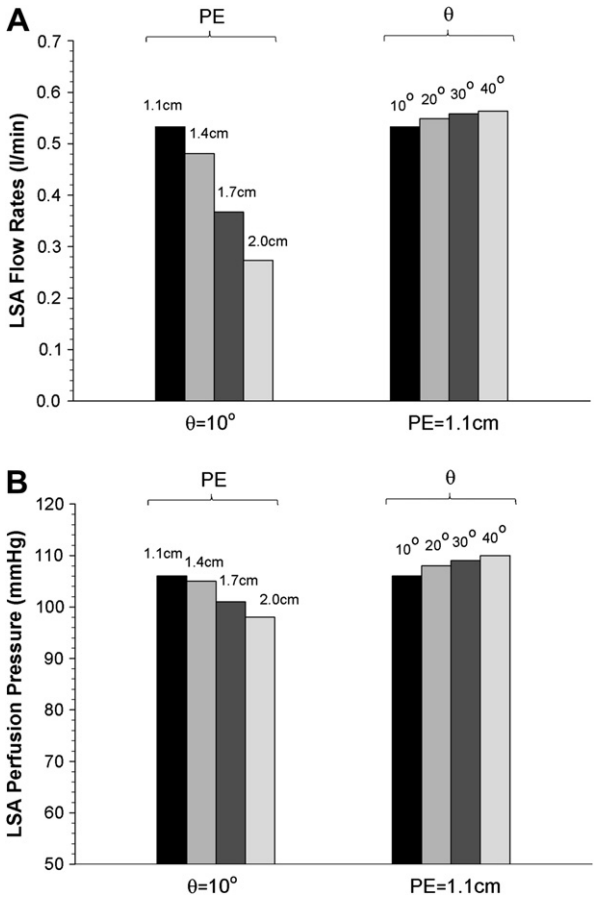

Fig 8. Volumetric flow rates **(A)** and blood perfusion pressure **(B)** through the left subclavian artery (*LSA*) over the cardiac cycle. For the model without the endograft, flow rate and blood perfusion are 0.55L/min and 116 mm Hg. *PE,* Protrusion extension.

values of θ (top three models in Fig 6). The longer PE of the TASG obstructs the antegrade blood flow, resulting in proximal hypertension.

At peak systole, comparison of blood velocity streamlines for the investigated varying degrees of malapposition reveals that as both geometric parameters increase, the number of vortices increases, which is associated with low blood velocity (high stagnation pressure) in the proximal luminal surface of the endograft (Fig 7). It was also observed that the blood flow velocity is low close to the distal TASG wall protrusion for the models with highest θ and PE values (18 cm/s for the model with PE = 1.1 cm and θ = 40 degrees and 25 cm/s for the model with PE = 2.0 cm and θ = 10 degrees).

Fig 8 shows the volumetric flow rates and perfusion pressures through the LSA over the cardiac cycle for the investigated geometries. Flow rates to the LSA are reduced markedly as the PE increases (Fig 8, *A*). Specifically, a reduction of flow to 0.27 L/min for the model with PE = 2.0 cm and θ = 10 degrees from 0.55 L/min without an endograft was observed. Additionally, a reduction of the peak systolic pressure into the LSA was found for the models with different PE compared with the model without an endograft (116 mm Hg) as shown in Fig 8, *B.* The TASG angulation did not alter significantly either flow rates or perfusion pressures to the LSA.

DISCUSSION

To our knowledge, this study is the first application of FSI modeling to investigate the mechanics of hemodynamic consequences of TASG malapposition and collapse. We evaluated the relevant hemodynamic and mechanical forces exerted on various, realistic geometries of endograft protrusions to assess the potential causative factors leading to hemodynamic disturbances and collapse. The present study demonstrates that, within the confines of the investigated geometric parameters, adverse clinical events, such as elevated transmural pressure, TASG deformation at peak systole, reduced distal blood flow, and reduced perfusion pressure, are associated with excessive PE.

Obstruction of the aorta from an intact TASG protruding into the arch is a complication of TASG placement that can lead to several complications, including reperfusion of the injured aortic segment, distal end-organ malperfusion syndrome, proximal hypertension, left upper extremity ischemia, and endoleaks. The results presented here suggest that a more pronounced proximal TASG protrusion is the main contributing factor to the onset of these adverse clinical events. Excessive PE results in reduced blood flow rate and perfusion pressure through the LSA, which could lead to distal end-organ malperfusion, left upper extremity ischemia, and proximal hypertension. Ueda et al[8] found a high risk of type Ia or II endoleaks with increasing length of the "bird beak," a result that is likely associated with the nearly steady flow in the wedge-shaped gap between the graft and aortic wall, as shown by our finding on blood flow streamlines. The TASG angulations appeared to play a secondary role compared with PE because blood flow rate and pressure perfusion to the LSA changed slightly.

Our data indicate that a marked PE configuration leads to an increased transmural pressure gradient across the protruded TASG wall, a load that would portend endograft infolding. This occurrence is likely due to higher dynamic and static pressures on the undersurface of the protruded TASG and cantilevering the proximal stent graft off the lesser curve of the distal arch. The stiffness of an endograft accounts for the resistance to such cantilevering effects. Angulation of the TASG appears to play a secondary role in the increase of transmural pressure likely owing to a lower cantilevering effect, and this offers less resistance to the flowing blood. In the setting of excessive PE, increased transmural pressure is also associated with reduced flow and perfusion pressure to the LSA, which portend TASG infolding. Transmural pressure across TASG wall protrusion may be considered a critical factor for collapse. The proximal anchorage system,[10,14,15] the radial force generated by the devices, and the ability of the endograft to accommodate

the compliance of the aorta (which may reach 17% between systole and diastole) are other important considerations to the mechanism of collapse.[27]

There are limitations to this study inherent to numerous anatomic and device-related variables that are not evaluated in this computational model, such as degree of oversizing, migration, and radial force of an endograft; migration; permeability; arch angulation and morphology; and material fatigue. The results of this study are limited to the confines of the studied variables because it did not fully evaluate the full spectrum of angulation and PE combinations. Furthermore, the results of this study may not be applicable to other endografts because different devices have different radial force and other biomechanical properties. Despite these limitations, the present computational FSI framework represents a valid tool to quantify the relevant hemodynamic loads acting on the proximal protrusion of thoracic stent grafts into the aortic arch, which are responsible for mechanisms underlying stent graft collapse.

CONCLUSIONS

Length of endograft PE and degree of angulation both can severely alter the hemodynamic forces acting on the proximal protrusion of the TASG, portending aortic coarctation and collapse. Excessive PE appears to have more adverse hemodynamic effects than angulation on the TASG. These findings may be considered in the clinical decision-making process for identification of patients with high propensity for collapse and for possible preemptive intervention, either by endovascular means or by open conversion.

AUTHOR CONTRIBUTIONS

Conception and design: SP, OD, JC, KP, DV
Analysis and interpretation: SP, JC, DV
Data collection: SP, OD, JC
Writing the article: SP, JC, DV
Critical revision of the article: SP, OD, JC, KP, DV
Final approval of the article: SP, OD, JC, KP, DV
Statistical analysis: Not applicable
Obtained funding: Not applicable
Overall responsibility: DV, JC
SP and JC contributed equally to this work.

REFERENCES

1. Melissano G, Civilini E, Bertoglio L, Setacci F, Chiesa R. Endovascular treatment of aortic arch aneurysms. Eur J Vasc Endovasc Surg 2005;29:131-8.
2. Criado FJ, Clark NS, Barnatan MF. Stent graft repair in the aortic arch and descending thoracic aorta: a 4-year experience. J Vasc Surg 2002;36:1121-7.
3. Go MR, Barbato JE, Dillavou ED, Gupta N, Rhee RY, Makaroun MS, et al. Thoracic endovascular aortic repair for traumatic aortic transection. J Vasc Surg 2007;46:928-33.
4. Celis RI, Park SC, Shukla AJ, Zenati MS, Chaer RA, Rhee RY, et al. Evolution of treatment for traumatic thoracic aortic injuries in a single institution. J Vasc Surg 2012;56:74-80.
5. Makaroun MS, Dillavou ED, Wheatley GH, Cambria RP, Gore TAG Investigators. Five-year results of endovascular treatment with the Gore TAG device compared with open repair of thoracic aortic aneurysms. J Vasc Surg 2008;47:912-8.
6. Cho JS, Haider SEA, Makaroun MS. Endovascular therapy of thoracic aneurysms: Gore TAG trial results. Semin Vasc Surg 2006;19:18-24.
7. Hinchliffe RJ, Krasznai A, SchultzeKool L, Blankensteijn JD, Falkenberg M, Lonn L, et al. Observations on the failure of stent-grafts in the aortic arch. Eur J Vasc Endovasc Surg 2007;34:451-6.
8. Ueda T, Fleischmann D, Dake MD, Rubin GD, Sze DY. Incomplete endograft apposition to the aortic arch: bird-beak configuration increases risk of endoleak formation after thoracic endovascular aortic repair. Radiology 2010;255:645-52.
9. Riesenman PJ, Farber MA, Fulton JJ. Endograft malapposition in the distal aortic arch resulting in functional coarctation. Vasc Endovasc Surg 2007;41:533-6.
10. Tadros RO, Lipsitz EC, Chaer RA, Faries PL, Marin ML, Cho JS. A multicenter experience of the management of collapsed thoracic endografts. J Vasc Surg 2011;53:1217-22.
11. Shukla AJ, Jeyabalan G, Cho JS. Late collapse of a thoracic endoprosthesis. J Vasc Surg 2011;53:798-801.
12. Go MR, Siegenthaler MP, Rhee RY, Gupta N, Makaroun MS, Cho JS. Physiologic coarctation of the aorta resulting from proximal protrusion of thoracic aortic stent grafts into the arch. J Vasc Surg 2008;48:1007-11.
13. Bandorski D, Bruck M, Gunther HU, Manke C. Endograft collapse after endovascular treatment for thoracic aortic disease. Cardiovasc Intervent Radiol 2010;33:492-7.
14. Canaud L, Alric P, Desgranges P, Marzelle J, Marty-Ane C, Becquemin JP. Factors favoring stent-graft collapse after thoracic endovascular aortic repair. J Thorac Cardiovasc Surg 2010;139:1153-7.
15. Sze DY, Mitchell RS, Miller DC, Fleischmann D, Frisoli JK, Kee ST, et al. Infolding and collapse of thoracic endoprostheses: manifestations and treatment options. J Thorac Cardiovasc Surg 2009;138:324-33.
16. Jonker FH, Schlosser FJ, Geirsson A, Sumpio BE, Moll FL, Muhs BE. Endograft collapse after thoracic endovascular aortic repair. J Endovasc Ther 2010;17:725-34.
17. Muhs BE, Balm R, White GH, Verhagen HJM. Anatomic factors associated with acute endograft collapse after Gore TAG treatment of thoracic aortic dissection or traumatic rupture. J Vasc Surg 2007;45:655-61.
18. Zhang W, Herrera C, Atluri SN, Kassab GS. Effect of surrounding tissue on vessel fluid and solid mechanics. J Biomech Eng 2004;126:760-9.
19. Dur O, Coskun ST, Coskun KO, Frakes D, Kara BL, Pekkan K. Computer aided patient specific coronary artery graft design improvements using CFD coupled shape optimizer. Cardiovasc Eng Technol 2011;2:35-47.
20. Pekkan K, Dur O, Sundareswaran K, Kanter K, Fogel M, Yoganathan A, et al. Neonatal aortic arch hemodynamics and perfusion during cardiopulmonary bypass. J Biomech Eng 2008;130:061012.
21. Sundareswaran KS, Pekkan K, Dasi LP, Whitehead K, Sharma S, Kanter KR, et al. The total cavopulmonary connection resistance: a significant impact on single ventricle hemodynamics at rest and exercise. Am J PhysiolHeart Circ Physiol 2008;295:H2427-35.
22. Dur O, DeGroff CG, Keller BB, Pekkan K. Optimization of inflow waveform phase-difference for minimized total cavopulmonary power loss. J Biomech Eng 2010;132:031012.
23. Li ZH, Kleinstreuer C. Blood flow and structure interactions in a stented abdominal aortic aneurysm model. Med Eng Phys 2005;27:369-82.
24. Li Z, Kleinstreuer C. Analysis of biomechanical factors affecting stent-graft migration in an abdominal aortic aneurysm model. J Biomech 2006;39:2264-73.
25. Rosero EB, Peshock RM, Khera A, Clagett GP, Timaran CH. Sex, race, and age distributions of mean aortic wall thickness in a multiethnic population-based sample. Circulation 2009;120:S463-4.
26. Raghavan ML, Vorp DA. Toward a biomechanical tool to evaluate rupture potential of abdominal aortic aneurysm: identification of a finite strain constitutive model and evaluation of its applicability. J Biomech 2000;33:475-82.
27. Steinbauer MG, Stehr A, Pfister K, Herold T, Zorger N, Topel I, et al. Endovascular repair of proximal endograft collapse after treatment for thoracic aortic disease. J Vasc Surg 2006;43:609-12.

Submitted Apr 24, 2012; accepted Sep 19, 2012.